This is a pre-print of the article:

Bianchi, F. D. and O. Gomis-Bellmunt. "Droop control design for multi-terminal VSC-HVDC grids based on LMI optimization". In: *Proc. of the 50th Conference on Decision and Control (CDC2011)*. Orlando, USA, 2011. DOI: 10.1109/CDC.2011.6161070.

DOI: 10.1109/CDC.2011.6161070

IEEEXplore Digital Library: http://ieeexplore.ieee.org/xpl/articleDetails.jsp?arnumber=6161070

Droop control design for multi-terminal VSC-HVDC grids based on LMI optimization

Fernando D. Bianchi and Oriol Gomis-Bellmunt

***Abstract*— The paper addresses the control of multi-terminal high voltage direct current (HVDC) networks with voltage source converters (VSCs). A general model is presented in order to describe the behavior of the multi-terminal VSC-HVDC networks in any possible operating condition. Based on this model, we propose a systematic design procedure for computing a decentralized static output feedback (SOF), the so-called droop control, with the aim of controlling the DC voltages. The design procedure is reduced to solving a convex optimization problem with linear matrix inequalities (LMIs). A four-terminal VSC-HVDC grid is use to illustrated the application of the proposed procedure.**

I. INTRODUCTION

The need for increasing the wind power production is fostering the research on offshore wind farms. In these facilities, the power captured by each turbine is concentrated in a common point and then conducted by submarine cables to the onshore substations connected to the main transmission system. Recent studies have concluded that for long distances the most appropriate option for the power transmission from the offshore wind farms to the coast is by high voltage direct current (HVDC) links [1]. This fact has led to a renewed interest in the HVDC grids and especially in the study of the stability and the voltage control.

The stability of HVDC grids have been widely studied [2], [3]. However, HVDC grids in the context of wind farm exhibit different characteristics and especially new control alternatives [4]. In wind power applications, an HVDC transmission results in a multi-terminal network where its terminals are connected to voltage source converters (VSCs) [5]. These converters permit to transfer the power from the wind farms to the AC grids where the consumes are connected. The role of control in these multi-terminal networks is to maintain the DC voltage almost stable and also to attenuate any oscillations produced by the change in the incoming power and by faults in the AC grids [4].

In general, in these multi-terminal HVDC grids, a decentralized proportional control, known as droop control, is employed to fulfil the specifications on the DC voltage behavior. Only a few works have addressed the control of these multi-terminals [4], [6]. The objective of this paper is to propose a systematic procedure to compute the droop gains ensuring stability and minimizing the effect of disturbances on the DC voltage. The proposed design is cast as a static output feedback (SOF) problem based on an $\mathcal{L}_2$ criterion expressed as a convex optimization problem with linear matrix inequalities (LMIs).

This work was supported by the *Ministerio de Ciencia e Innovación* under the projects ENE2009-08555 and DPI2008-00403

F.D. Bianchi and O. Gomis-Bellmunt are with the Catalonia Institute for Energy Research (IREC), Power Electronics and Electric Power Grids Dept., Jardins de les Dones de Negre 1, 2ª pl., 08930 Sant Adrià de Besòs, Barcelona, Spain, {fbianchi,ogomis}@irec.cat

O. Gomis-Bellmunt is also with CITCEA, Departament d'Enginyeria Elèctrica, Universitat Politècnica de Catalunya, Av. Diagonal, 647, Pl. 2. 08028 Barcelona, Spain

II. MULTI-TERMINAL VSC-HVDC GRIDS

A typical multi-terminal VSC-HVDC network is shown in Figure 1. These systems can be modelled as an interconnection of nodes and branches. The nodes represent the VSCs and the joints of several cables at intermediate points. The branches are the cables linking the nodes. The converters on both sides of the multi-terminal grid are nodes injecting power (wind farm side) and extracting power (AC grid side). The converters on the wind farm side (WFCs) are called power input nodes and the converters on the AC grid side (GSCs) are the power output nodes.

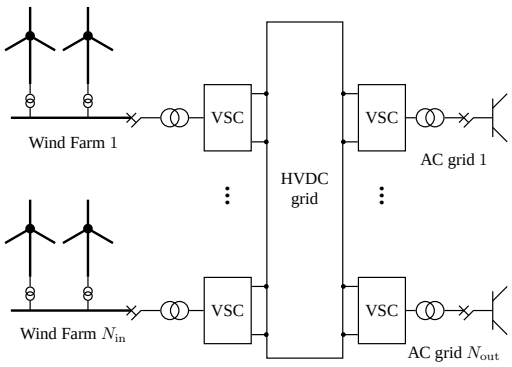

Fig. 1. Typical HVDC multi-terminal network

For the present analysis, it is sufficient to consider average models for the VSCs. In this case, the converter is modelled as three AC sources and one DC source plus a capacitor [7]. The currents and voltages on the AC side are connected with the DC side variables through the power transferred from one side to the other. The control of the VSCs consists of two feedback loops, an inner loop controlling the currents and an outer loop regulating the DC voltage. The dynamic of the inner loop can be considered much faster than the outer loop and therefore it can be neglected in this study. As a consequence, the VSCs will be represented as sources that inject or extract current according to a current-voltage characteristic given by the local control of the VSCs [5].

The WFCs present three operating modes as can be seen in Figure 2 [5]. The normal operation mode, where the

converters transfer all the power coming from the wind farm, the VSC behaves as a current source keeping the power injected into the grid constant. In Figure 2, it can be seen several characteristics for several power values, where $P_{\max}$ denotes the converter power limit. The hyperbolic sector of the curves corresponds to the normal operation. At high DC voltages, the VSC maintains the voltage almost constant by means of a proportional control law, commonly known as droop control. The current is limited when it reaches the maximum value I_{wfH}. This characteristic for a generic node k is summarized as follows

$$I_k = \begin{cases} K_k(E_{\mathrm{wfH},k} - E_k), & E_{\mathrm{wfL},k} < E_k < E_{\mathrm{wfH},k}; \\ P_k/E_k, & E_k \leq E_{\mathrm{wfL},k} \ \& \ I_k < I_{\mathrm{wfH},k}; \\ I_{\mathrm{wfH},k}, & I_k \geq I_{\mathrm{wfH},k}. \end{cases} \tag{1}$$

with $k = 1, \ldots, N_{\mathrm{in}}$. Notice that the limit between the droop and normal modes ($E_{\mathrm{wfL},k}$) depends on the power level delivered by the wind farm. In Figure 2, the operation modes are indicated for the case of $60\%P_{\max}$ injected into the grid (thick line). The shadow area indicates the range where the DC voltages must remains, *i.e.*, $E_k \in [\underline{E}_{\mathrm{wf}}, \overline{E}_{\mathrm{wf}}]$

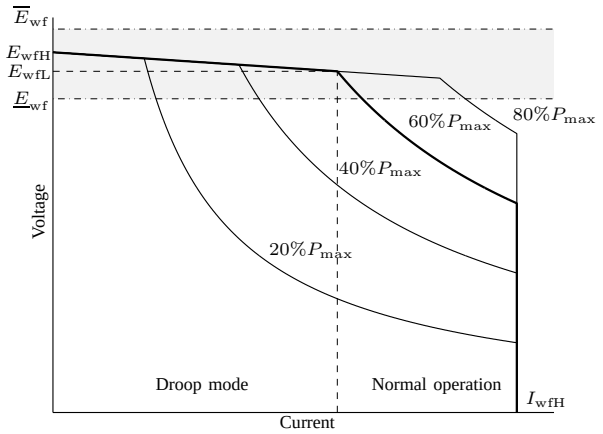

Fig. 2. Current-voltage characteristic of a wind farm converter for several values of power delivered by the wind farm

The GSCs present two operating modes. In this case, the normal operation corresponds to the droop control of the DC voltage. The second operating mode, current limitation, is applied when the current reaches the converter limit given by

$$I_{\mathrm{gsH},k} = \frac{P_{\max}}{E_k} = \frac{\sqrt{3}V_{AC}\cos\theta}{E_k} I_{AC}^{\max}, \tag{2}$$

where V_{AC} and $I_{AC}^{\max}$ are the AC voltage and the AC current, respectively. The current-voltage curve is illustrated in Figure 3 and obeys the following expression

$$I_k = \begin{cases} K_k(E_k - E_{\mathrm{gsL},k}), & I_k < I_{\mathrm{gsH},k}; \\ I_{\mathrm{gsH},k}, & \text{otherwise.} \end{cases} \tag{3}$$

with $k = 1, \ldots, N_{\mathrm{out}}$. The shadow area indicates the range $[\underline{E}_{\mathrm{gs}}, \overline{E}_{\mathrm{gs}}]$ of the acceptable DC voltage values. Commonly, the converters on the AC grid side work in droop control mode. However, the converter may enter in the current limitation mode during severe voltage faults in the AC grid. In this circumstance, the AC voltage (V_{AC}) drops and the capacity of the converter to transfer power is reduced. From (2), it is clear that a voltage sag of 50% causes a reduction of the current limit I_{gsH} in 50%, which in turn reduces the normal operation area. This situation is also illustrated in Figure 3 (thin line).

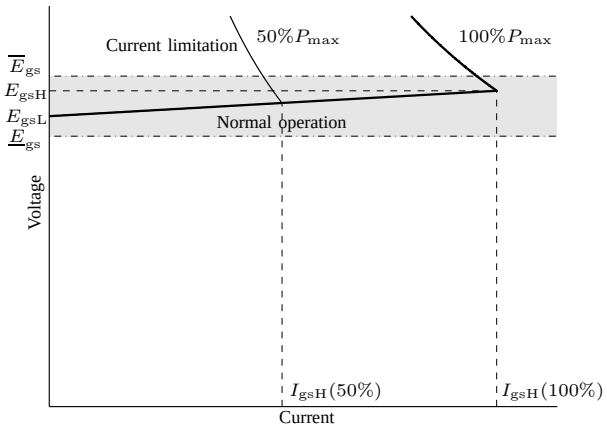

Fig. 3. Current-voltage characteristic of a grid side converter. The thin line shows the characteristic under a voltage sag of 50%

The rest of the multi-terminal VSC-HVDC is basically an RLC circuit where each cable is substituted for an equivalent π-circuit. The capacitors of the VSC models are included in this RLC circuit. In order to eliminate unnecessary states, capacitors in parallel are substituted for an equivalent one of value

$$C_k = \sum_{j=1}^{N} C_j. \tag{4}$$

The interconnection of nodes and branches after combining parallel capacitors results in passive electrical network with N_{in} power input nodes and N_{out} power output nodes. A current source is connected to each terminal. These current sources, obeying one of the current-voltage characteristic previously described, model the effect of the local control of the VSCs. An example of this kind of circuits can be seen in Figure 4, which represents a four-terminal VSC-HVDC grid with two wind farms transferring power to two AC grids.

The state-space representation of the equivalent electrical network can be obtained from the following expressions.

- The voltage at an input/output node k is given by

$$\dot{E}_k = \frac{\alpha_k}{C_k}(I_k - \sum_{j \in \mathcal{J}_{\mathrm{io}}} I_{L_j}), \quad k = 1, \ldots, N_{\mathrm{in}} + N_{\mathrm{out}} \tag{5}$$

  where the set $\mathcal{J}_{\mathrm{io}}$ includes the indexes of all branches converging to the node k and α_k is a parameter that takes the value 1 in case of a power input node and -1 in case of a power output node.

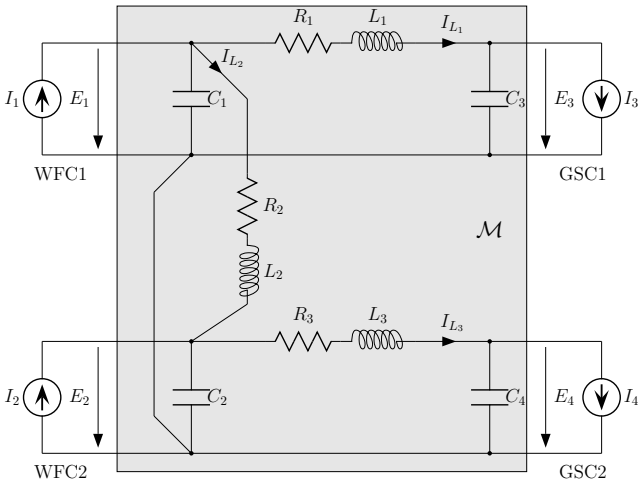

Fig. 4. Equivalent circuit of a four-terminal VSC-HVDC network

- The voltage at an intermediate node k is given by

$$\dot{E}_k = \frac{1}{C_k}\Big(\sum_{j\in\mathcal{J}_{\rm in}} I_{L_j} - \sum_{j\in\mathcal{J}_{\rm out}} I_{L_j}\Big), \quad k = 1,\dots,N_{\rm int} \tag{6}$$

  where $\mathcal{J}_{\rm in}$ is the set of indexes of all branches with currents flowing to the node k and $\mathcal{J}_{\rm out}$ is the set of indexes with currents flowing from the node k.
- The current in a branch l between the nodes k and m is given by

$$\dot{I}_{L_l} = \frac{1}{L_l}(-R_l I_{L_l} + E_k - E_m), \quad l = 1,\dots,N_{\rm br} \tag{7}$$

Then, defining the state vector as

$$x = [E_1,\cdots,E_{(N_{\rm in}+N_{\rm out})}, E_{(N_{\rm in}+N_{\rm out}+1)},\dots, E_{(N_{\rm in}+N_{\rm out}+N_{\rm int})}, I_{L_1},\cdots,I_{L_{N_{\rm br}}}]^T, \tag{8}$$

the electrical network has the state-space representation

$$\mathcal{M}: \begin{cases} \dot{x} = Ax + B_q q, \\ p = C_p x, \end{cases} \tag{9}$$

where

$$A = \begin{bmatrix} 0 & 0 & A_{13} \\ 0 & 0 & A_{23} \\ A_{31} & A_{32} & A_{33} \end{bmatrix}, \quad B_q = \begin{bmatrix} B_1 \\ 0 \\ 0 \end{bmatrix}, \quad C_p = \begin{bmatrix} I \\ 0 \\ 0 \end{bmatrix}^T,$$

with A_{13}, A_{23}, A_{31}, A_{32}, A_{33} and B_1 matrices obtained from the previous electrical equations.

III. CONTROL DESIGN PROCEDURE

In this section, we provide a procedure to design the droop control gains on both side of the multi-terminal network under multiple operating conditions. In normal operation, the WFCs inject power into the multi-terminal and the GSCs regulate the DC voltage. This implies that only the controllers on the AC grid side are active. However, this control configuration changes under different operating conditions. For example, under a voltage fault on the AC grid, the roles of the converters may be reversed and the WFCs become responsible for maintaining the DC voltage within limits whereas the controllers on the AC grid side remain inactive. As a consequence, the control design must ensure stability and performance for a time varying system, actually the control must deal with a time-varying system since the changes in the control configuration occur in very short periods of time. On the other hand, the control must be decentralized since each local control can not use the voltage measured at other nodes. The distance among nodes makes unreliable the use of the voltage at other nodes in a control law.

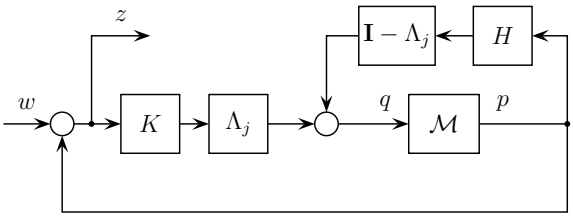

Fig. 5. Proposed control loop representation for the multi-terminal VSC-HVDC grid

Here, we propose the scheme depicted in Figure 5 to represent the changes in the operating modes of the multi-terminal VSC-HVDC networks. In this scheme, all outputs are fed back into the multi-terminal network $\mathcal{M}$; however, the only feedback gains to be designed are those associated to the droop control (the matrix K). The other feedback paths are caused by the relation between the current and the voltage when the power handled by the converter is constant.

The main idea consists in representing the nonlinear relation between the current and the voltage at each power node as

$$I_k = \delta_k E_k,$$

where δ_k is a time-varying parameter taking values in the sector $[\underline{\delta}_k, K_k]$. Therefore, the multi-terminal network can be modelled as the LPV system

$$\mathcal{F}_u(\Delta, \mathcal{M})$$

where $\mathcal{F}_u$ denotes the upper linear fractional interconnection and $\Delta = \mathrm{diag}(\delta_1,\dots,\delta_{(N_{\rm in}+N_{\rm out})})$.

As the resultant model is actually an affine LPV system, to establish stability and performance is sufficient to evaluate the closed loop system at the vertex of the polytope $\mathbf{\Delta} = [\underline{\delta}_1, K_1]\times\cdots\times[\underline{\delta}_{N_{\rm in}+N_{\rm out}}, K_{N_{\rm in}+N_{\rm out}}]$. Therefore, for control design purpose, the input to the multi-terminal $\mathcal{M}$ is

$$q = K\Lambda_j(w+p) + H(\mathbf{I}-\Lambda_j)p \tag{10}$$

where $\mathbf{I}$ is the identity matrix,

$$K = \mathrm{diag}(K_1,\dots,K_{(N_{\rm in}+N_{\rm out})})$$

is the droop gain to be determined and

$$H = \mathrm{diag}(\underline{\delta}_1,\dots,\underline{\delta}_{(N_{\rm in}+N_{\rm out})}).$$

The matrix Λ_j is defined as

$$\Lambda_j = \text{diag}(\Lambda_{1,j}, \ldots, \Lambda_{(N_{\text{in}}+N_{\text{out}}),j}),$$

where

$$\Lambda_{k,j} = \begin{cases} 1, & \text{if droop is applied at the node } k; \\ 0, & \text{otherwise.} \end{cases} \quad (11)$$

This matrix determines the control configuration, *i.e.*, which nodes are in droop control and which are just injecting or extracting power without voltage control. For example, in normal operation, where the WFCs inject into the multi-terminal HVDC network all the wind power available and the GSCs are in droop control to regulate the DC voltage, the matrix results

$$\Lambda = \text{diag}(\underbrace{0, \ldots, 0}_{N_{\text{in}}}, \underbrace{1, \ldots, 1}_{N_{\text{out}}}).$$

This configuration changes if, for instance, a voltage fault occurs in the AC grid. This provokes that some of the converters on the AC grid side enter in current limitation and some of the WFCs enters in droop control. If all WFCs are in droop control and the GSCs in current limitation, the matrix Λ takes the form of

$$\Lambda = \text{diag}(\underbrace{1, \ldots, 1}_{N_{\text{in}}}, \underbrace{0, \ldots, 0}_{N_{\text{out}}}).$$

There are $2^{(N_{\text{in}}+N_{\text{out}})}$ possible configurations. Nevertheless, this number can be reduced with an analysis to determine the possible cases. This depends to a large extent on the voltages $E_{\text{wfL},k}$ and $E_{\text{gsL},k}$ which are set in accordance to a power distribution study which is out of the scope of this paper [5].

Then, the closed loop system is governed by

$$\begin{aligned} \dot{x} &= A_{cl,j}x + B_w w, \\ z &= C_z x + D_{zw} w, \end{aligned} \quad (12)$$

where

$$A_{cl,j} = \begin{bmatrix} B_1(K\Lambda_j + H(\mathbf{I} - \Lambda_j)) & 0 & A_{13} \\ 0 & 0 & A_{23} \\ A_{31} & A_{32} & A_{33} \end{bmatrix},$$

$$B_{w,j} = \begin{bmatrix} (B_1\Lambda_j)^T & 0 & 0 \end{bmatrix}^T, \quad C_z = \begin{bmatrix} \mathbf{I} & 0 & 0 \end{bmatrix},$$

$D_{zw} = \mathbf{I}$, with $j = 1, \ldots, N$ ($N \leq 2^{(N_{\text{in}}+N_{\text{out}})}$). Due to the changes in the matrix Λ_j, the multi-terminal HVDC grid represented by (12) is actually a time-varying system.

The purpose of the droop control is to maintain almost constant the DC voltages in spite of disturbances caused by the change in the wind power and the faults in the AC grid. This objective must be fulfilled even though when some converters change from one operating mode to other. This objective will be stated in the form of the $\mathcal{L}_2$ criterion

$$\max_{w \neq 0} \frac{\|z\|_2}{\|w\|_2} < \gamma. \quad (13)$$

A result similar to the Bounded Real Lemma permits to formulate the previous performance criterion as constraints on the droop gain K [8]. Using this result, the system satisfies the performance condition (13) if there exists a positive definite matrix P such that

$$\begin{bmatrix} PA_{cl,j} + (\star) & PB_{w,j} & C_z^T \\ \star & -\gamma I & D_{zw}^T \\ \star & \star & -\gamma I \end{bmatrix} < 0, \; \forall\, j = 1, \ldots, N \quad (14)$$

where < 0 denotes negative definite and $\star$ the matrix symmetric elements. Notice that in order to guarantee stability and performance against changes in the operating modes, the Lyapunov matrix P must be common to each system j.

The droop gain can be computed replacing the closed loop matrices $A_{cl,j}$ in (14). This leads to a decentralized static output feedback problem which requires solving a non-convex optimization problem. Nevertheless, since B_w is a full column rank matrix, the gain computation can be reduced to a convex problem (at the expense of some conservatism) by defining the Lyapunov matrix as

$$P = \begin{bmatrix} P_1 & 0 \\ 0 & P_2 \end{bmatrix},$$

with $P_1 = \text{diag}(p_1, \ldots, p_{(N_{\text{in}}+N_{\text{out}})})$ and P_2 a symmetric matrix of dimension $(N_{\text{br}} + N_{\text{int}}) \times (N_{\text{br}} + N_{\text{int}})$ [9]. From the previous discussion, it is straightforward to prove the following result.

Theorem 3.1: The decentralized proportional control K stabilizes the system (9) and ensures (13) if there exist matrices $P_1 = \text{diag}(p_1, \ldots, p_{(N_{\text{in}}+N_{\text{out}})}) > 0$, $P_2 = P_2^T > 0$ and $V = \text{diag}(v_1, \ldots, v_{N_{\text{in}}+N_{\text{out}}})$ such that

$$\begin{bmatrix} P(A + B_1H(I - \Lambda_j)) + V\Lambda_j + (\star) & V\Lambda_j & C_z^T \\ \star & -\gamma\mathbf{I} & D_{zw}^T \\ \star & \star & -\gamma\mathbf{I} \end{bmatrix} < 0 \quad (15)$$

for all $j = 1, \ldots, N$. Once P_1 and V are computed, the droop gain can be obtained from

$$K = VP_1^{-1}.$$

IV. EXAMPLE

The application of Theorem 3.1 is illustrated with the simple four-terminal VSC-HVDC grid that is shown in Figure 4. It consists of two offshore WFCs and two onshore GSCs. The values of the parameters are listed in Table I. The four-terminal grid has two power input nodes, two power output nodes and three branches representing the cables linking the converters.

Using the expression (5) at each power input/output node and (7) in the three branches, the following differential equations can be obtained

$$\dot{E}_1 = \frac{1}{C_1}(I_1 - I_{L_1} - I_{L_2}), \quad (16)$$

$$\dot{E}_2 = \frac{1}{C_2}(I_2 - I_{L_3} - I_{L_2}), \quad (17)$$

$$\dot{E}_3 = \frac{-1}{C_3}(I_3 - I_{L_1}), \quad (18)$$

$$\dot{E}_4 = \frac{-1}{C_4}(I_4 - I_{L_3}), \quad (19)$$

TABLE I

PARAMETER OF THE FOUR-TERMINAL EXAMPLE

Grid parameters	Value
Line resistance R_1 and inductance L_1	0.50 Ω, 5.0 mH
Line resistance R_2 and inductance L_2	0.25 Ω, 2.5 mH
Line resistance R_3 and inductance L_3	0.40 Ω, 4.0 mH
Capacitances C_k $(k = 1, \ldots, 4)$	150 μF
Rated line current i_L^{rtd}	667 A
Rated input current i_k^{rtd}	667 A
Converter rated power P_k	100 MW
Rated DC voltage E_k	150 kV
Reference voltage E_0	145 kV

$$\dot{I}_{L_1} = \frac{1}{L_1}(-R_1\, I_{L_1} + E_1 - E_3), \tag{20}$$

$$\dot{I}_{L_2} = \frac{1}{L_2}(-R_2\, I_{L_2} + E_1 - E_2), \tag{21}$$

$$\dot{I}_{L_3} = \frac{1}{L_3}(-R_3\, I_{L_3} + E_2 - E_4), \tag{22}$$

There are four capacitors and three inductor; therefore, the variables E_1, E_2, E_3, E_4, I_{L_1}, I_{L_2} and I_{L_3} are sufficient to completely define the state of the system, *i.e.*,

$$x = [E_1\ E_2\ E_3\ E_4\ I_{L_1}\ I_{L_2}\ I_{L_3}]^T.$$

From this previous definition and the equations (16)–(22), the open loop matrix in the state-space representation (9) results

$$A = \begin{bmatrix} 0 & 0 & 0 & 0 & -\frac{1}{C_1} & -\frac{1}{C_1} & 0 \\ 0 & 0 & 0 & 0 & 0 & -\frac{1}{C_2} & -\frac{1}{C_2} \\ 0 & 0 & 0 & 0 & -\frac{1}{C_3} & 0 & 0 \\ 0 & 0 & 0 & 0 & 0 & 0 & -\frac{1}{C_4} \\ \frac{1}{L_1} & 0 & -\frac{1}{L_1} & 0 & -\frac{R_1}{L_1} & 0 & 0 \\ \frac{1}{L_2} & -\frac{1}{L_2} & 0 & 0 & 0 & -\frac{R_2}{L_2} & 0 \\ 0 & \frac{1}{L_3} & 0 & -\frac{1}{L_3} & 0 & 0 & -\frac{R_3}{L_3} \end{bmatrix},$$

$$B = \begin{bmatrix} \frac{1}{C_1} & 0 & 0 & 0 \\ 0 & \frac{1}{C_2} & 0 & 0 \\ 0 & 0 & -\frac{1}{C_3} & 0 \\ 0 & 0 & 0 & -\frac{1}{C_4} \\ 0 & 0 & 0 & 0 \\ 0 & 0 & 0 & 0 \\ 0 & 0 & 0 & 0 \end{bmatrix}.$$

There are $N_{\text{in}} + N_{\text{out}} = 2 + 2 = 4$ converters therefore there are $2^{(N_{\text{in}}+N_{\text{out}})} = 16$ possible control configurations. The application of the proposed procedure given by Theorem 3.1 for the 16 possible Λ_j produces the following droop gain

$$K = \text{diag}(-0.1333, -0.1333, 0.1333, 0.1333).$$

with a performance level of $\gamma = 2.00$, where the output z was weighted with the function

$$W_{z,j}(s) = \frac{s/0.5 + 1}{s/50 + 1} \cdot \text{diag}\left(\beta_{1,j}, \beta_{2,j}, \beta_{3,j}, \beta_{4,j}\right),$$

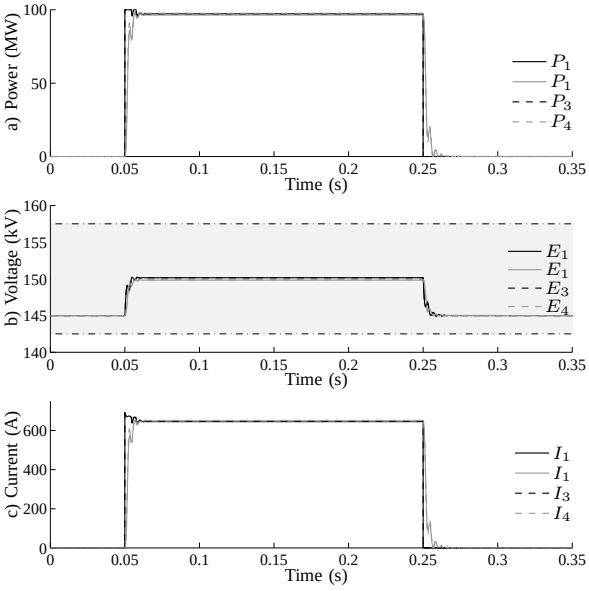

Fig. 6. Simulations corresponding to a change in the power injected into the grid by the WFCs

The parameters $\beta_{i,j}$ was set at 0.01 for the outputs corresponding to the nodes without droop control and at 0.02 for the outputs with control. The optimization problem was solved with the free available software Sedumi [10] and Yalmip [11].

The droop gain computed with the proposed procedure were evaluated by simulation. The first scenario analyzed consists in two simultaneous changes in the power injected into the multi-terminal VSC-HVDC grid by the WFCs. The powers at the input nodes vary from 0 MW to the rated value 100 MW at 0.05 s and return to 0 MW at 0.25 s. Figure 6a shows the evolution of the power at each converter. The solid lines correspond to the power injected by the WFCs and the dashed lines to the power extracted by the GSCs. The DC voltages are shown in Figure 6b, the shadow area indicates the range ($\pm 5\%$ of rated voltage 150 kV) where the DC voltage must remain. Notice that the voltage at the four terminal never exceed the limits. The DC voltages stay at 145 kV during the period where the power flow is zero since there is no voltage drop in the grid resistances. Once the power input increases, the DC voltages move toward a new voltage equilibrium. The currents flowing through each converters are displayed in Figure 6c.

The second scenario considered is two voltage faults in the AC grids. Initially, the four converters are working at normal operation, *i.e.*, the WFCs are injecting all wind power available and the GSCs are regulating the DC voltages. At 0.05 s, a three phase voltage sag of 90% deep of the nominal AC values occurs at the AC grid connected to the GSC3. At the same time, another voltage sag of 80% deep is applied to the grid connected to the GSC4. The both sags last 0.2 s. The simulation results are shown in Figure 7. It can be observed that the powers and the currents at the grid side

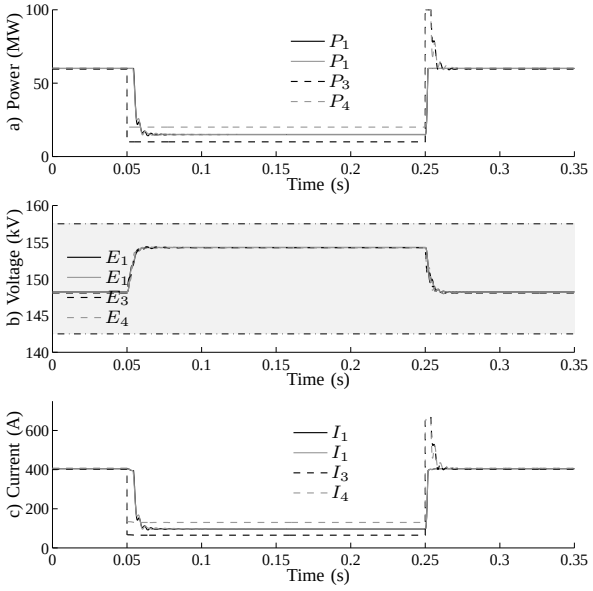

Fig. 7. Simulations corresponding to voltage sags in the AC grids

(I_3 and I_4 and P_3 and P_4, respectively) fall at 0.05 s due to the voltage sags in the AC grids. When the WFC voltages exceed 154 kV, the corresponding converters start to applied droop control in the DC grid, reducing the power injected into the grid from 100 MW to 20 MW. (Figure 7a). The DC currents also decrease during the voltage sag due to the power reduction caused by the droop control in the WFCs (Figure 7c). Notice that the disconnection of the system due to over-voltage was avoided during the fault. The voltages at all terminal rose as consequence of the grid side converter operated in current limitation mode. Nevertheless, the DC voltages never left the shadow area delimited by the voltage limits.

The change of operating modes is clearer in Figure 8, where the behavior of the system is represented in the current-voltage plane (For sake of clarity, only the voltages and the currents of WFC1 and GSC3 are depicted, similar results can be observed in the others converters). Initially, WFC1 and GSC3 are in normal operation (point **A**). After the voltage faults in the AC grids, GSC3 enters in current limitation mode (point **C**) whereas WFC1 remains in normal operation but the voltage E_1 begins to rise. Once E_1 reaches 154 kV (point **B**), the WFC1 enters in droop control mode. Both converters stay in this configuration until the voltage fault vanishes (point **D**). Once the AC voltage recovers the rated values, the GSC3 returns to normal operation (point **E**), causing an initial increment of the current I_3 until the system reaches the final operating point **A**. Whereas, the variables in WFC1 return to the initial point **A** along the same path than they followed to reach **D**.

V. CONCLUSIONS

The voltage regulation of multi-terminal VSC-HVDC networks requires the design of decentralized static controller that ensures stability and performance under changes in the operating conditions. The synthesis of these decentralized controllers has been cast a SOF problem. The particular structures of the system and the control have been exploited to propose a relaxation in order to convexify the synthesis procedure and thus simplifying the computation of the static feedback. As a result, the decentralized static controller can be computed by solving a convex optimization problem with LMI constraints. A general switched description of multi-terminal VSC-HVDC networks has also been introduced with the aim of describing the multi-terminal under any possible operating conditions. With this formulation, the designed static control stabilizes and provides certain performance level under any operating condition of the multi-terminal VSC-HVDC grid.

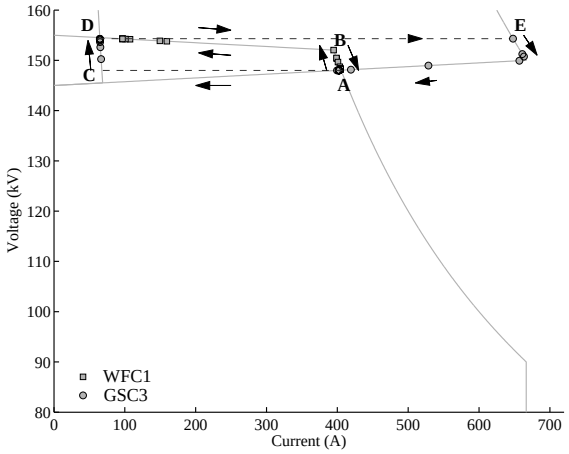

Fig. 8. Simulations corresponding to a voltage sag in the AC grids in the current-voltage plane

REFERENCES

[1] T. Ackermann. Transmission systems for offshore wind farms. *IEEE Power Engineering Review*, 22(12):23–27, Dec. 2002.

[2] P. Kundur. *Power System Stability and Control*. McGraw-Hill Professional, 1994.

[3] J. Machowski, J. Bialek, and J. Bumby. *Power system dynamics and stability*. Wiley, 1997.

[4] J. Liang, O. Gomis-Bellmunt, J. Ekanayake, and N. Jenkins. Control of multi-terminal VSC-HVDC transmission for offshore wind power. In *Proc. of the 13th European Conf. Power Electronics and Applications (EPE '09)*, pages 1–10, 2009.

[5] O. Gomis-Bellmunt, J. Liang, J. Ekanayake, and N. Jenkins. Voltage-current characteristics of multiterminal HVDC-VSC for offshore wind farms. *Electrical Power Systems Research*, 81(2):440–450, 2011.

[6] E. Prieto-Araujo, F. Bianchi, A. Junyent-Ferré, and O. Gomis-Bellmunt. Methodology for droop control dynamic analysis of multi-terminal VSC-HVDC grids for offshore wind farms. *IEEE Trans. on Power Delivery*, 2011.

[7] G. Zhang, Z. Xu, and Y. Cai. An equivalent model for simulating VSC based HVDC. In *Proc. of the IEEE/PES Transmission and Distribution Conf. and Exposition*, volume 1, pages 20–24, 2001.

[8] B. Lu and F. Wu. Switching LPV control designs using multiple parameter-dependent Lyapunov functions. *Automatica*, 40(11):1973–1980, 2004.

[9] M Mattei. Robust multivariable PID control for linear parameter varying systems. *Automatica*, 37(12):1997–2003, 2001.

[10] J Sturm. *Primal-dual interior point approach to semidefinite programming*. Phd thesis, Tilburg University, Dept. of Econometrics, 1997.

[11] J. Lofberg. YALMIP: A toolbox for modeling and optimization in MATLAB. In *Proc. of the CACSD Conference*, Taipei, Taiwan, 2004.